AN ABSTRACT OF THE THESIS OF

Susan H. Elliott for the degree of Master of Science in Water Resource Engineering presented on October 12, 2016.

Title: Physical modeling of the feedbacks between a Reed Canarygrass (*Phalaris arundinacea*) patch, hydraulics, and bedform evolution.

Abstract approved:

_____

Desirée D. Tullos

Reed Canarygrass (RCG) is an aggressive invader in aquatic ecosystems that swiftly modifies the environment and decreases biodiversity. A physical model was used to investigate the mechanisms by which RCG spreads. Experimental trials were implemented to examine feedbacks between a mid-channel patch of the flexible RCG, hydraulics, and bedform evolution as level of submergence increases and plant deflection occurred. The objectives of the study were (1) to examine feedbacks in wake and turbulence length scales and depositional patterns as plant submergence changes, (2) to investigate how the wake characteristics vary with depth and (3) to identify possible mechanisms for RCG expansion in the channel based on the observed positive and negative feedbacks and frontal area analysis. It was found that streamlined patch expansion is promoted at low submergence levels through the positive feedbacks of greater wake zone deposition and a

long wake length scale. At low submergence depth, greater lateral scour served as a negative feedback for lateral patch expansion, inhibiting growth next to the patch. As submergence increases, stem deflection begins to occur and vertical shear turbulence is introduced in the wake zone in the upper portion of the water column. This turbulence shortens wake length scales and diminishes wake zone deposition, resulting in a negative feedback for streamlined patch expansion. However, a positive feedback for lateral patch expansion was seen at medium submergence due to diminished lateral velocities and near-bed stem deflection near the bed. Understanding of these feedbacks helps to inform management priorities and anticipate the geomorphic invasion-induced impacts such as diminished habitat diversity, decreased flood conveyance and channel incision.

Physical Modeling of the Feedbacks Between a Reed Canarygrass (*Phalaris arundinacea*) Patch, Hydraulics, and Bedform Evolution.

by
Susan H. Elliott

A THESIS

submitted to

Oregon State University

in partial fulfillment of
the requirements for the
degree of

Master of Science

Presented October 12, 2016
Commencement June 2017

Master of Science thesis of Susan H. Elliott presented on October 12, 2016

APPROVED:

Major Professor, representing Water Resource Engineering

Director of the Water Resources Graduate Program

Dean of the Graduate School

I understand that my thesis will become part of the permanent collection of Oregon State University libraries. My signature below authorizes release of my thesis to any reader upon request.

Susan H. Elliott, Author

ACKNOWLEDGEMENTS

The author expresses sincere appreciation to her advisor, Dr. Desirée Tullos, and her committee, Dr. Jack Istok and Dr. Chad Higgins, for their guidance, encouragement and support. She also expresses gratitude to those who helped in the construction of the flume and providing essential supplies: Robert Predosa, Jeff Gent, the Hydrophiles, the Hydrogeology lab, Dr. John Selker's lab and Cara Walter. And, finally, she would like to express her deepest gratitude for the support in flume design and construction and general positive energy provided by her husband, Adam Elliott.

TABLE OF CONTENTS

LIST OF FIGURES

LIST OF FIGURES (continued)

Figure Page

LIST OF TABLES

1 Introduction

Invasive vegetation species can cause severe negative impacts on fluvial landscapes. The dominance and control over biogeomorphic processes occurs through positively-enforcing feedbacks, i.e., mechanisms that induce biogeomorphic change that lead to other mechanisms that in turn lead to vegetation expansion (Ehrenfeld, 2010). While previous research has identified detailed vegetation-induced feedbacks within a natural channel (Bouma et al., 2007; Curran & Hession, 2013; Heidi M. Nepf, 2012a; Tsujimoto, 1999), few studies have focused specifically on feedbacks with invasive vegetation species (Fei, Phillips, & Shouse, 2014; Lavergne & Molofsky, 2004). To effectively manage invasive species in river systems, it is important to identify the particular biogeomorphic feedbacks that drive individual species expansion.

Reed Canarygrass (RCG), *Phalaris arundinacea*, is one example of a non-native grass species that thrives in aquatic ecosystems where it has dramatically modified the landscape throughout North America (Apfelbaum, Sams, & others, 1987; Lavergne & Molofsky, 2004). As a riparian plant, RCG thrives along stream banks where it has been found to spread into the wetted channel (Barnes, 1999; Henry & Amoros, 1996). The plant's high architectural plasticity and large annual seed yield allow the grass to withstand high flow

velocities, use the river as a seed dispersal corridor, and colonize with a greater success rate than most native species (Apfelbaum et al., 1987; Lavergne & Molofsky, 2004). RCG's highest germination rates have been found in water-saturated soils (Coops & Van Der Velde, 1995; Kellogg, Bridgham, & Leicht, 2003) while anoxia tolerant rhizome shoots also continue to survive during prolonged flooding events (Apfelbaum et al., 1987). Simultaneously, RCG can also survive during periods of drought and through large fluctuations of seasonal temperatures (Lavergne & Molofsky, 2004). As a result of these biological characteristics, RCG often forms a dense monocrop by aggressively outcompeting other species (Barnes, 1999; Paveglio & Kilbride, 2000; Washington State Department of Ecology, n.d.).

RCG's tenacity to thrive in aquatic systems can have swift impacts upon the morphology and biodiversity of the fluvial ecosystem. The plant meets the definition of an invasive geomorphological ecosystem engineer (Corenblit et al., 2011) due to its ability to negatively alter the flow regime through diminished flood conveyance and channel incision. The organism also facilitates niche construction whereby long-term impacts of environmental modifications modifies other species' niches (Odling-Smee, Feldman, & Laland, 2003). For instance, by migrating into a river channel and constricting flow, RCG degrades fish habitat and diminishes overall biodiversity (Washington State Department of Ecology, n.d.). Identification of the

particular hydraulic and bedform feedbacks of the invasive vegetation within the channel is essential to understanding and controlling further expansion.

Previous flume and field studies have identified the spatial distribution of deposition and erosion around vegetation patches, the hydrodynamics of the flow field surrounding these patch, and the influence of vegetation's biomechanical structure on hydraulics and bedform (Corenblit, Tabacchi, Steiger, & Gurnell, 2007; Curran & Hession, 2013; Folkard, 2011a; Gurnell, Bertoldi, & Corenblit, 2012; Heidi M. Nepf, 1999, 2012b; Tsujimoto, 1999; C. A. Wilson, Hoyt, & Schnauder, 2008). This work has highlighted three key feedbacks between plants, hydraulics, and deposition.

First, vegetation patches alter patterns of sediment transport that have been linked to nutrient transmission and mechanisms for expansion. Fine sediment particle deposition has been observed in the vegetation wake region due to lowered velocities passing through the patch canopy (Chen, Ortiz, Zong, & Nepf, 2012a). This fine material is higher in nutrients and therefore has been identified as a positive feedback for patch expansion (Gurnell et al., 2001). Deposited sediment also encourages seed and organic material collection (Abt, Clary, & Thornton, 1994; Corenblit et al., 2007), further promoting streamlined expansion behind vegetation patches. Regions of scour next to the patch have been identified as a negative feedback for lateral patch expansion (Ortiz, Ashton, & Nepf, 2013; Kaj Sand-Jensen & Mebus,

1996). These regions have a coarser grain size and less nutrient-rich sediment (Corenblit et al., 2007).

Second, the wake zone length and location of high turbulent kinetic energy influences sediment transport patterns and bedform evolution. The wake zone length (L), defined as the distance from the downstream edge of the patch to the onset of the von Kármán vortex street (Ball, Stansby, & Alliston, 1996), has been studied for rigid, emergent vegetation patches (Chen, Ortiz, Zong, & Nepf, 2012b; Follett & Nepf, 2012; Ortiz et al., 2013; Zong & Nepf, 2010, 2011b). The wake region is created as vegetation absorbs upstream flow (U_0), reducing velocities through the patch and deflecting flow laterally. A low velocity (U_W) region is created along the centerline within the wake behind the patch, while two high-velocity shear layers develop lateral to the patch (U_{LAT}). The wake zone region has been further discretized into two regions. The steady wake zone (L_{ST}) extends until velocity downstream of the patch begins to increase. The wake recovery region (L_{RE}) extends from L_{ST} until velocity returns to upstream velocity (U_0). The full wake zone length is thus $L_{ST} + L_{RE}$. Lateral to the wake region, the two lateral shear layers merge some distance downstream and induce a region of elevated turbulence known as the von-Kármán vortex street. The vortex street has been observed and mapped in flumes with vegetation patches using dye tracers (Zong & Nepf, 2011a) and simulated in numerical models (Nicolle & Eames, 2011). These visualizations

revealed the distance each lateral shear layer traveled without mixing with the wake region velocity (Zong & Nepf, 2011b). Previous research defined wake region turbulence scales for emergent and submerged vegetation patches (Follett & Nepf, 2012; H.M. Nepf & Vivoni, 2000; Nicolle & Eames, 2011; Zong & Nepf, 2010). Turbulent kinetic energy (TKE) was diminished in the low velocity wake region and begins to increase with the onset of the vortex street. The turbulence length scale, L_{TKE}, is the region where TKE increases behind the patch, ending at the peak TKE value. This value marks the formation of the vortex street forms (Ortiz et al., 2013). Turbulence and impacted velocities alter sediment transport feedbacks. Turbulent eddies both lateral to the patch and behind the wake region promote sediment mobility and erosion (Cellino & Lemmin, 2004). The resuspension of sediment due to near-bed turbulence also inhibits deposition, creating a negative feedback for patch expansion (Follett & Nepf, 2012). The lower velocity wake region promotes deposition for a positive feedback for patch expansion (Chen et al., 2012b).

Third, the degree of submergence, and therefore the biomechanical properties that lead to stem deflection for flexible vegetation, is the dominant control on wake flow dynamics (Chen, Jiang, & Nepf, 2013). Submergence is also dependent upon flow velocity for flexible vegetation that pronates with increasing flow (Luhar & Nepf, 2013). This pronation, or deflection, changes

the frontal area exposed to flow and thus further alters the density of vegetation, which is a primary driver in bedform evolution at the local scale (Curran & Hession, 2013; Hickin, 1984). Density is most commonly calculated using number of plants or stems per bed area (Chen et al., 2012b; Zong & Nepf, 2010, 2011a, 2011b). However, real vegetation often has varying stem diameters and blades or fronds that can greatly increase the flow absorption within the patch. For instance, when compared to two native plants, the invasive RCG was found to have a higher potential to interrupt flow measured by total frontal area despite having the lowest density (plants m^{-2}) of all three species (Martinez & McDowell, 2016). However, the total foliage area of flexible vegetation decreases when subjected to flow because the blades become more streamlined with increasing velocity (C. A. Wilson et al., 2008). These dynamic properties make determining vegetation density challenging. The variability in structure of real vegetation, specifically plant flexibility, has led to differences in approaches for characterizing frontal area in a system with varying velocity (Green, 2005; Kaj Sand-Jensen, 2003; Sukhodolov, 2005). The changing plant structure also introduces a third velocity shear layer over the canopy (Folkard, 2005, 2011b). Canopy scale turbulence develops at the top of the vegetation, inducing a turbulence layer within the water column and a vertical recirculation zone in the wake region (Chen et al., 2012a; Folkard, 2011b), leading to the negative feedback for patch expansion

due to increase in turbulence and decrease in deposition. In natural channels, fluctuating water levels can induce a range of flow blockage areas over time.

These examples of strong biogeomorphic feedbacks in natural channels make river systems more vulnerable to the geomorphic influences of invasive species (Fei et al., 2014). However, little is known about the impact of RCG (Lavergne & Molofsky, 2004) and other invasive species on geomorphological processes (Fei et al., 2014). This study investigated the feedbacks between a mid-channel patch of Reed Canarygrass, hydraulics and bedform evolution as level of submergence increased and plant deflection occurs. The specific objectives of the study were (1) to examine feedbacks in wake and turbulence length scales and depositional patterns as plant submergence changes, (2) to investigate how the wake characteristics vary with depth and (3) to identify possible mechanisms for RCG expansion in the channel based on the observed positive and negative feedbacks. It was hypothesized that RCG would behave similarly to rigid, emergent vegetation during low submergence, where deposition occurs within the wake region and scour occurs lateral to the plant, thus optimizing streamlined expansion and inhibiting lateral expansion. As submergence depth increases and vegetation becomes partially deflected, it is predicted that vertical shear over deflected stems will increase turbulence in the wake zone and reduce wake zone

length, thus providing a negative feedback for deposition within the wake zone and streamlined expansion.

2 Materials and Methods

2.1 Experimental set-up

Physical modeling was conducted in a 10-m-long by 0.46-m-wide flume that recirculated water but not sediment. The flume bed slope was 0.0007 and a downstream weir controlled the flow depth. Sediment was isolated within a 0.1 m deep and 3.2 m long sediment pit and a 0.05 m deep and 3.0 m long sediment runway (Figure 1). Sediment was modeled using a plastic composite material with a specific gravity of 1.5 g/cm^3 and a d_{50} of 1.4 mm. This density falls within a typical range for materials commonly used in physical geomorphology models (Julien, Pierre Y., 2002). The lighter material was chosen to produce sediment movement at the lower velocities necessary for Froude similitude. Calculations were performed to verify that sediment entrainment would occur at model flow velocities (see Appendix).

A circular RCG patch with a 10 cm diameter (D) was fixed in the center of the cross section located 4.6 m downstream from the head of the flume (Figure 2). The patch diameter was chosen based on the percentage of total flume width area (22% of the total 46 cm width). Previous experiments found

minimal influence of the walls with patch percentages of total width ranging from 18% (Follett & Nepf, 2012) to 35% (Ortiz et al., 2013; Zong & Nepf, 2011b) of the width of the flume.

Patch density is described in two ways: without-blade foliage area and with-blade foliage area. These two calculations provide the minimum and maximum frontal areas (a_1 and a_2 respectively) of RCG, which can be compared with previous vegetation patch studies. Additionally, the minimum and maximum solid volume fractions, ϕ_1 and ϕ_2 respectively, were calculated as another way to compare RCG patch density to previous studies.

The threshold between sparse and dense vegetation in a circular patch has been defined using solid volume fraction,

$$\phi = \pi a d/4, \quad \text{(Eq. 1)}$$

where frontal area per unit volume (a_1) is described as

$$a_1 = nd, \quad \text{(Eq. 2)}$$

with n as the stems per bed area and d as the stem diameter (Zong & Nepf, 2010).

For the without-blade foliage area, stem diameter is used as the plant area characteristic, consistent with previous studies that investigated reedy vegetation using rigid cylinders as surrogate as a means to simplify plant characteristics (Chen et al., 2012b; Follett & Nepf, 2012). The RCG patch in

this study consisted of 20 stems in a circular array with an average diameter (d) of 0.29 cm, resulting in a density (n) of 0.25 cm^{-1} (Table 1). The minimum solid volume fraction (ϕ_1) was 0.02. Sparse, intermediate and dense vegetation is defined as $\phi < 0.05$, $0.05 < \phi < 0.1$, and $\phi > 0.15$ respectively (Nicolle & Eames, 2011; Poggi, Katul, & Albertson, 2004). Thus, without taking foliage area into account, the patch is classified having a sparse density.

For the with-blade foliage area, stem diameter and the average blade area per plant was used as the plant characteristic area to determine maximum frontal area (a_2) and maximum solid volume (ϕ_2). Frontal area per unit volume (a_2) was calculated by:

$$a_2 = n(\frac{A_0}{h}) \quad \text{(Eq. 3)}$$

where A_0 is the total projected frontal area of the dry plant and h is total water depth for partially submerged plants. This method is appropriate as an estimation for maximum potential flow blockage since it accounts for all possible frontal area that could be subjected to flow. Using this method frontal area (a_2) is found to be 1.14 cm^{-1} and 1.13 cm^{-1} for low and medium submergence trials respectively, averaging to 1.13 cm^{-1}. The solid volume fraction (ϕ_2) is found to be 0.26 for both low and medium submergence trials. For the with-blade foliage area, the patch is characterized as a dense canopy.

The patch density was kept constant in all trials. To preserve the plant's flexural rigidity and biomechanical properties, real plants were used in flume trials, thus resulting in a 1:1 geometric scale to surveyed vegetation in the field. A vegetation height of 45 cm was chosen to fit within the flume and also allow for partial submergence during medium depth trials. While shorter than the mean height of surveyed plants (99 cm), the modeled height did fall within the 5% - 95% confidence range (43.1 cm to 168 cm respectively) for heights of surveyed plants (see Appendix).

Model flows were determined using a reference reach on the Chiloquin River in southeastern Oregon and scaled using Froude similitude. The reference site was chosen based on an abundance of riparian Reed Canarygrass stands and available channel survey data. Depth was used as a characteristic length scale, h, in the Froude similitude equation since it is varied between trials. A reference velocity of 35 cm/s was selected from surveyed velocities at the edge of wetted channel during lower summer flows. A surveyed prototype depth of 43 cm and a model depth of 14 cm were used to determine a model upstream velocity of 20 cm/s. Actual upstream velocities achieved during experimental trials ranged from 19.2 cm/s to 21.0 cm/s (Table 2). Uniform flow in the upstream region was confirmed for each trial prior to vegetation being placed in the flume. Verification of uniform flow was made using a HACH flow meter to collect velocity measurements at 0.2

and 0.6 of total water depth, h, at four lateral locations spaced 0.3 m apart along the length of the flume in the streamwise direction. Experiments were run between 4.5 – 6 hours.

2.2 Velocity measurements

Velocity measurements were collected using three Sontek 10-MHz Acoustic Doppler Velocimeters (ADVs) in a downward-facing position. The instruments were fixed to a movable cart such that velocities were measured 5 cm above the bed for the low submergence depth trial and both 5 cm and 10 cm above the bed for the medium submergence trial. The ADV sampling volume was located 5 cm below the probe. Velocity data were collected every 10 cm in the longitudinal direction within the experimental zone at three lateral positions: patch centerline, edge of patch and lateral to patch (Figure 2). Velocity data were collected every 5 cm in the longitudinal direction for the near-patch region (x =15 cm – 25 cm). Velocity was recorded at each location at a sampling rate of 25 Hz for 240 s.

Velocity data were processed using WinADV post-processing software (Wahl, n.d.). Data with less than a 70% correlation and a signal-to-noise ratio less than 5 dB were removed. Phase space threshold despiking and acceleration spike filter were used to filter out spikes in the velocity data (Goring & Nikora, 2002). Velocity data with vegetation interference, as noted

during data collection, were removed. An upstream velocity, U_0, at x = -40 cm was used to normalize velocity values for each trial (Figure 2).

Turbulence length scales were determined using the following methods. Turbulent kinetic energy, TKE, per unit mass was calculated using (Pope, 2000)

$$TKE = \sqrt{(\overline{u'^2} + \overline{v'^2} + \overline{w'^2})} \quad \text{(Eq. 4)}$$

where *u', v'* and *w'* are the temporally averaged velocities for each directional component x, y and z respectively. The TKE is thus the square root of the mean of the deviations from the mean for each individual velocity component. TKE values were then non-dimensionalized using the mean of the upstream velocity values (U_0).

2.3 Bed surface measurements

Erosion and depositional patterns and change in volume of sediment stored on the bed were measured using LiDAR imagery. A Faro 3D Focus laser scanner was inverted from the instrument platform to scan the bed. Before each experiment, vegetation was secured in foam and covered with 4-6 cm of sediment. The surrounding sediment was then leveled by eye. Four scans (*pre* experiment scans), positioned approximately 1 m apart along the length of the flume, were collected before water was introduced to the flume

(Figure 3). The scans were positioned around the sediment pit to maximize coverage and minimize shadowed regions within the experiment zone. After each experiment was completed, the flume was slowly drained overnight to minimize disturbance to the bedform. Once fully drained, vegetation was cut as close to the bed as possible without disturbing the bed and four *post* scans were collected.

LiDAR scans were processed with Leica Geosystem's Cyclone software (*Leica Cyclone*, n.d.) using surveyed total station data within the flume for geo-referencing. Each set of four *pre* and *post* scans were combined using target and cloud-to-cloud registration, resulting in a single *pre* and single *post* scan. Vegetation points from cut stems were manually removed from the *post* scan. LiDAR point clouds were transferred into ArcGIS and converted to raster format using the Spatial Analyst toolbox (*ArcGIS Desktop*, 2013). The *pre* scans were smoothed using aggregate and resample toolboxes. The smoothing was performed to mimic the initial smoothing that occurred with the first wave of water entering the flume. The resulting digital elevation models (DEMs) were used to perform DEM differencing by subtracting the *pre* scan from the *post* scan for each trial. Using the DEM of difference (DEMoD), net surface volume changes were calculated for each trial by isolating values above and below a zero datum and performing volume calculations on the subsequent terrain. Volumes above the zero datum of the DEMoD were

interpreted as deposition regions and volumes below the zero datum were interpreted as eroded regions. Laterally averaged deposition values were calculated at 125 locations longitudinally across the experimental zone.

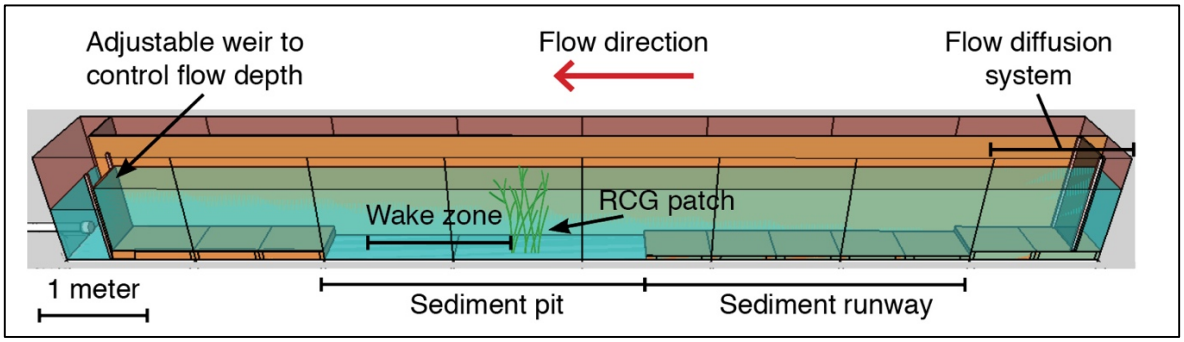

Figure 1: Flume model diagram. Flow is from right to left. Sediment is placed in the sediment runway and sediment pit. The experimental zone is located within the sediment pit area surrounding the RCG patch and extending downstream of predicted wake zone area. An adjustable weir at the downstream end of the flume is used to control depth between trials. Flow diffusion system location is pictured. Flow was diffused through large cobbles, screens and 30 cm-long diffusion tubes (not pictured). Flow diffusion was required to ensure a uniform upstream flow, U_0, entering the experimental zone.

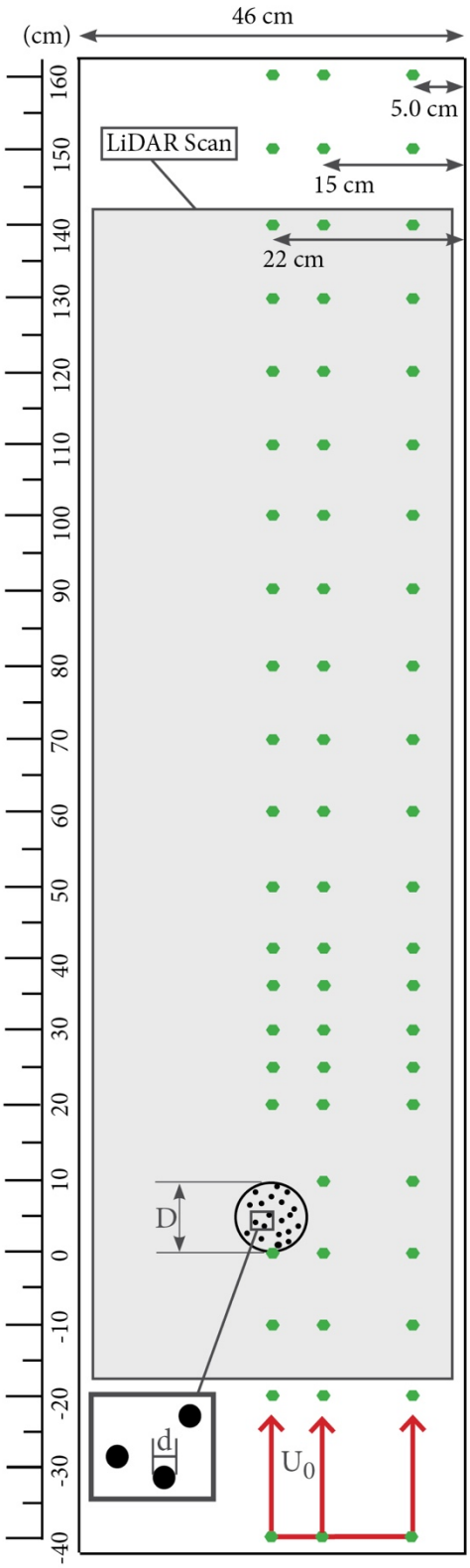

Figure 2: Experimental set-up diagram. Red arrow shows flow direction of upstream velocity U_0, measured using the average values at x = -40 cm. Velocity data were collected at the patch centerline (22 cm from right wall), at the patch edge (15 cm from right wall) and lateral to the patch (5 cm from right wall). Green points indicate locations where velocity data were collected when vegetation deflection did not interfere. Patch diameter D, was fixed at 10.1 cm and an average stem diameter of 0.29 cm was used for all calculations. Stems are shown in random array similar to placement during experimental trials. The grey box illustrates the LiDAR data extents. The experimental zone is defined from x = -0.20 m to 1.60 m, or from 0.20 m upstream of the vegetation patch to the end of the sediment pit.

Patch parameters	
d (cm)	0.29
D (cm)	10.1
n (stems cm^{-2})	0.25
a_1 (cm^{-1})	0.07
a_2 (cm^{-1})	1.14
ϕ_1	0.02
ϕ_2	0.26

Table 1: Summary of patch parameters for all trials. Stem diameter d (cm), patch diameter D (cm), minimum frontal area a_1 (cm^{-1}), maximum frontal area a_2 (cm^{-1}), patch density n (stems cm^{-2}), minimum solid volume fraction ϕ_1 and maximum solid volume fraction ϕ_1 are shown.

Experimental parameters								
Trial	**z (cm)**	**Flow rate (ft^3/s)**	**h (cm)**	**Duration (h)**	**U_0 (cm/s)**	**L_{ST} (cm)**	**L_{RE} (cm)**	**L_{TKE} (cm)**
Low	5	0.53	14	4	19.2	55	95	65
Medium	5	1.11	34	6.5	21.0	55	95	75
	10					65	>140	45

Table 2: Summary of experimental parameters for all trials. Height of measurement above the bed z (cm), flow rate as read on pump flow meter (ft^3/s), submergence depth h (cm), duration of experiment (h), upstream velocity (U_0), steady wake zone length L_{ST} (cm), wake recovery region length L_{RE} (cm), turbulent kinetic energy length scale L_{TKE} (cm), and net deposition (cm^3) in experimental zone. When length scale was beyond experimental zone a '>' symbol is used.

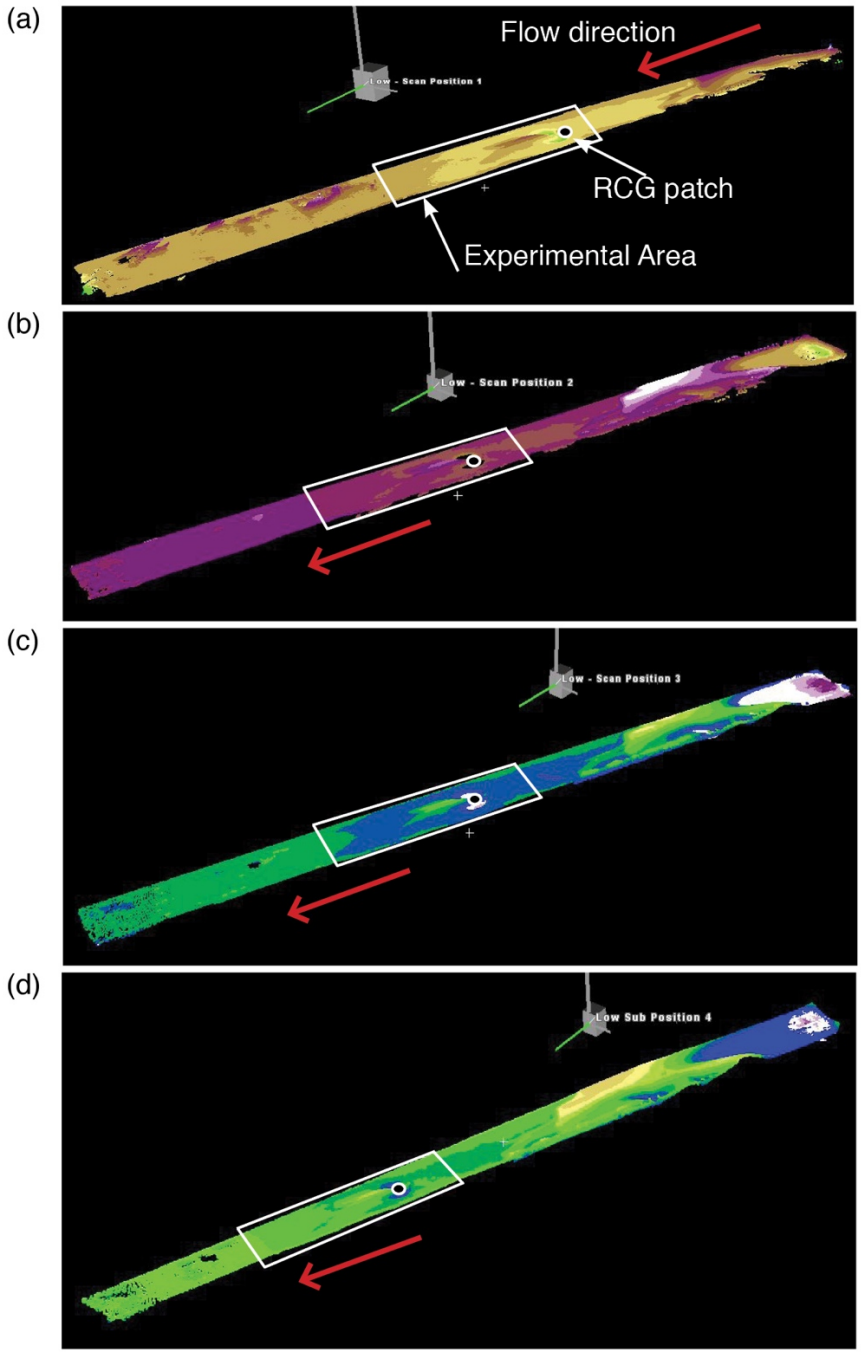

Figure 3: Example scan positions along flume in relation to patch location. Images show post-experiment scans of the low submergence trial. These scans were combined to create one robust post-experiment LiDAR point cloud that minimized any shadowing of bedform. Grey box is scanner location on instrument platform approximately 0.75 m above the bed. Scanner was placed in position 1(a) downstream of wake zone, position 2 (b) within wake zone, position 3 (c) upstream of vegetation patch, and position 4 (c) upstream of experimental zone. LiDAR point cloud for bed pre-processing is shown.

3 Results

3.1 Lateral velocities

Normalized velocities lateral to the patch (U_{LAT}, 5 cm from the right wall) vary between the low and medium submergence trials despite similar upstream velocities (U_0 = 19.2 cm/s and 21.0 cm/s respectively) (Figure 4). Normalized lateral velocities in the low trial were higher throughout the entire experimental zone than the medium trial, despite having the lower upstream velocity.

3.2 Low submergence trial

The low submergence depth trial shows clear formation of wake length scales, turbulence length scales, and patterns of sediment transport that are similar to rigid, emergent vegetation patches. The low depth trial shows a clear transition between L_{ST} to L_{RE} (Figure 5a), where the velocity values in the centerline behind the patch drop and then begin to rise again. This “dip” in velocity results from reduced velocity flowing through the patch, decreasing velocity downstream of patch, before lateral shear velocity layers rejoin, increasing velocity behind the patch. At x = 55 cm, L_{RE} begins and velocity increases for the wake recovery region. Here, TKE reaches a maximum at L_{TKE} (Figure 5a). L_{RE} ends when velocity reaches U_0 at x = 95 cm.

Laterally averaged deposition (Figure 5b) occurs primarily within the wake region between x = 29 cm to x = 95 cm. At the downstream extent of L_{ST}, x = 55 cm, deposition begins to increase, and further decreases after L_{TKE}, x = 65 cm. Finally, the end of the wake depositional zone ends at the end of the wake recovery region, L_{RE}.

The DEM for the low trial (Figure 6a) shows two regions of lateral scour on either side of the patch of nearly equal length downstream of the patch. Deposition downstream of the patch is organized as a ridgeline along the centerline of the patch, which splits into two ridgelines near the downstream extent of L_{TKE}, x = 64 cm, that move away from the centerline.

Profile images of the RCG patch at both low and medium submergence shows observed deflection patterns (Figure 7). Deflection due to velocity in the low trial was not observed and natural plant position was maintained.

3.3 Medium submergence trial

Results from the medium submergence depth trial produced similar patterns of wake and turbulence length scale as the low submergence depth trial at 5 cm above the bed. However, new patterns of turbulence and velocity were observed for velocity measurements located 10 cm above the bed. At 5 cm above the bed, a drop in the wake velocities can be seen (Figure 8a) that

defines the transition between the steady wake region, L_{ST}, to the wake recovery region, L_{RE}. L_{ST} and L_{RE} are the same lengths as the low submergence trial, 55 cm and 95 cm respectively, while L_{TKE} extends 10 cm farther downstream than L_{TKE} for the low trial to x=75 cm total. L_{TKE} also ends within the wake recovery region, similar to the low trial.

Wake region length scales measured at 10 cm above the bed show influence of the fully deflected vegetation (Figure 8b). Profile images of the patches for both submergence trials show minimal deflection in the low submergence trial (Figure 7a) and full deflection (submerged) for a portion of the RCG patch at medium submergence (Figure 7b). Approximately 75% of the RCG patch at this greater submergence level became deflected enough to be submerged just below the water surface behind the patch.

At 10 cm above the bed, the steady wake region L_{ST} is 65 cm long, which is 10 cm longer than L_{ST} at 5 cm above the bed for both the low and medium submergence trials (Figure 8b). Another notable difference between the two velocity measurement depths is the turbulence length scale, L_{TKE}, which is 20 cm shorter than L_{ST} for the velocities measured 10 cm above the bed, but was 20 cm longer than L_{ST} for the velocities nearer the bed. This early turbulence could be originating from the mixing of vertical flow over the fully deflected stems with wake zone velocities rather than originating from the two lateral regions of high velocity meeting behind the wake zone.

Furthermore, velocities measured at 10 cm above the bed do not return to upstream velocities (U_0), indicating that the length of the wake recovery region is greater than the experimental zone in the flume (>140 cm). This may also support continued disruption of flow due to deflected stems since velocities did return to upstream levels closer to the bed (5 cm above the bed) where less deflection occurred (Figure 8a).

Deposition and erosion patterns for the medium submergence depth diverged to some degree from the low submergence trial. First, deposition was observed in front of the patch in this trial (Figure 6b, Figure 8c), unlike the low submergence trial which showed a zero net lateral averaged deposition upstream of the patch. Upstream sediment transport patterns in the medium trial reveal that erosion (negative laterally averaged deposition) occurred between x = -176.8 cm to -88.4 cm where deposition continued until the stem-induced scour within and lateral to the RCG patch at x = 3.9 cm (Figure 9). The medium submergence depth upstream velocity (U_0) and velocities leading up to the RCG patch were nearly equal to those of the low submergence trial (0.03 cm/s average difference), but the discharge was higher due to an increase in depth.

Second, the deposition downstream of the RCG patch in the medium submergence trial is more irregular than the peak in downstream deposition in the low submergence trial (Figure 8c). This downstream net deposition region

contains two peaks. The first begins at x = 16 cm, which is 13 cm closer to the downstream edge of the patch than the low submergence trial where deposition began at x = 29 cm. This is likely due to less scour (and negative deposition values) lateral to the patch. Visually evident in the DEMs, the lateral scour region right of the patch in the medium submergence trial extends to approximately x = 17 cm, and the left scour region to approximately x = 14 cm (Figure 6b). The left and right regions of scour in the low submergence trial both extend to approximately x = 23 cm (Figure 6a).

Comparing the laterally averaged deposition in both trials, it is evident that the low trial caused greater scour within and near the downstream edge of the patch than the medium submergence trial (Figure 10). While total height of deposition between the two trials was nearly identical (approximately 0.13 m), wake deposition patterns varied in longitudinal position. In the medium submergence trial, the initial peak in deposition occurred before the initial peak in the low submergence trial. Additionally, a second peak in the medium trial occurred after the end of the deposition region in the low submergence trial.

Wake region length scales measured at both 5 cm and 10 cm above the bed do not follow patterns in deposition as they do in the low submergence trial (Figure 8c). At 5 cm above the bed, the steady wake length scale, L_{ST}, extends beyond the first peak in the depositional area and occurs

in a region of decreasing deposition (Figure 8a). This makes sense as velocities and TKE should be increasing after this point which both have been linked to an increase in sediment resuspension. At the same 5 cm measurement elevation above the bed, the peak in TKE marked by the turbulent length scale L_{TKE} occurs just before the second peak in deposition behind the patch. Downstream of this point, deposition does plateau and then decrease, although not immediately as it is expected with high turbulence. The end of the wake recover region, L_{RE}, occurs beyond the peak in TKE at x = 95 cm. This is the same total wake length as the low submergence depth. However, at medium submergence, deposition continues after for 22 cm farther downstream of the wake recovery region, indicating that deposition occurs even as upstream velocity levels are attained.

While velocity and turbulence measurements at 10 cm above the bed are farther above the bed, they provide insight into sediment resuspension and therefore may contribute toward depositional patterns. High levels of turbulence may maintain particles in suspension while regions of diminished velocity relative to upstream may promote particle deposition. At the peak in turbulence, L_{TKE}, at this elevation above the bed, deposition behind the patch is decreasing, possibly because more particles are remaining in suspension at 10 cm above the bed. The end of the steady wake region measured at 10 cm above the bed occurs in the trough of the two peaks in deposition behind

the patch. Between this point and the end of the experimental zone, velocities do not return to upstream flow levels possibly allowing more sediment particles to fall out of suspension. Patterns in deposition support this, as a second deposition peak occurs after L_{ST} and continues until beyond the end of the wake recovery region measured at 5 cm above the bed.

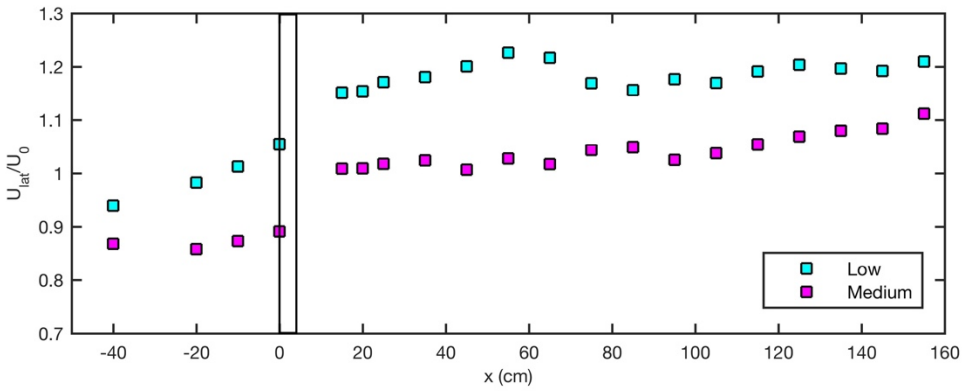

Figure 4: Normalized lateral velocity U_{LAT}/U_0 in the streamwise direction for low and medium submergence trials. Low submergence depth velocities shown in cyan and medium submergence depth velocities shown in pink. Lateral velocities taken 5 cm from the right wall at 5 cm elevation above the bed.

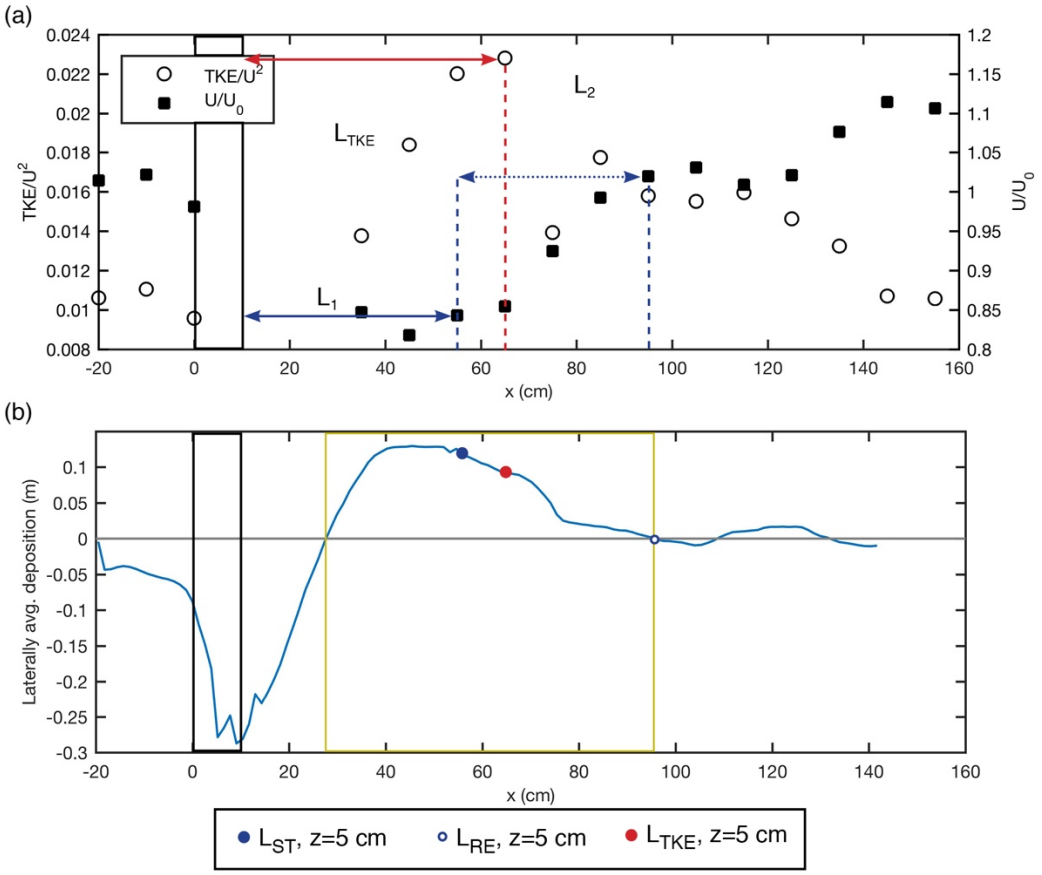

Figure 5: Low submergence depth trial flow field at 5 cm above the bed and laterally averaged deposition data. In (a) centerline velocities are normalized by upstream free-stream velocity values, U_0, and centerline TKE values are normalized by local velocity values. The patch location at x = 0 is shown with solid black lines in both plots. Steady wake length, L_{ST}, and wake recovery region length, L_{RE}, are shown with a solid dark blue arrow and a dotted dark blue arrow respectively. The turbulence length scale, L_{TKE}, is shown with a red arrow. Dotted vertical lines show the length along the streamwise direction, x. In (b) laterally averaged deposition across the experimental area is shown with the wake depositional region outlined in yellow box. A solid blue dot indicates the length scale L_{ST} along the streamwise direction, an open blue dot shows the length scale for L_{RE} and the red dot shows the length scale L_{TKE}.

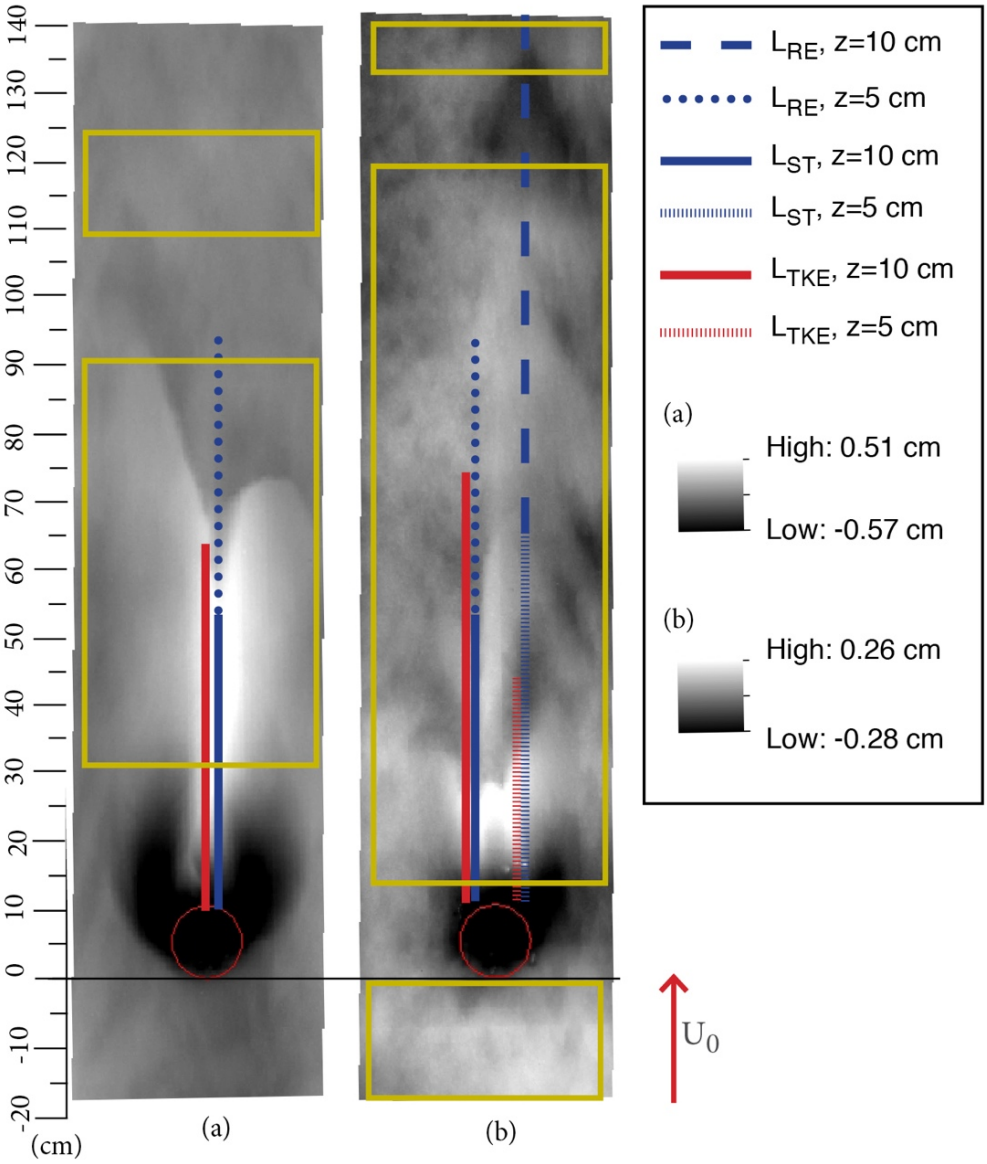

Figure 6: Digital elevation models (DEMs) for low and medium submergence trials with length scales and depositional regions shown. Low submergence trial DEM (a) and medium submergence trial DEM (b) are overlaid with turbulence length, L_{TKE} (red lines), steady wake region length, L_{ST} (solid blue lines), and wake recovery region length, L_{RE} (dotted blue lines) measured at 5 cm above the bed. In (b), length scales for measurements taken at 10 cm above the bed, L_{TKE} (hatched red line), L_{ST} (hatched blue line), and L_{RE} (dashed blue line), are also shown. All length scales measured along the centerline. Yellow boxes are areas of net laterally averaged deposition. Patch location shown as a red circle. U_0 shown with a red arrow.

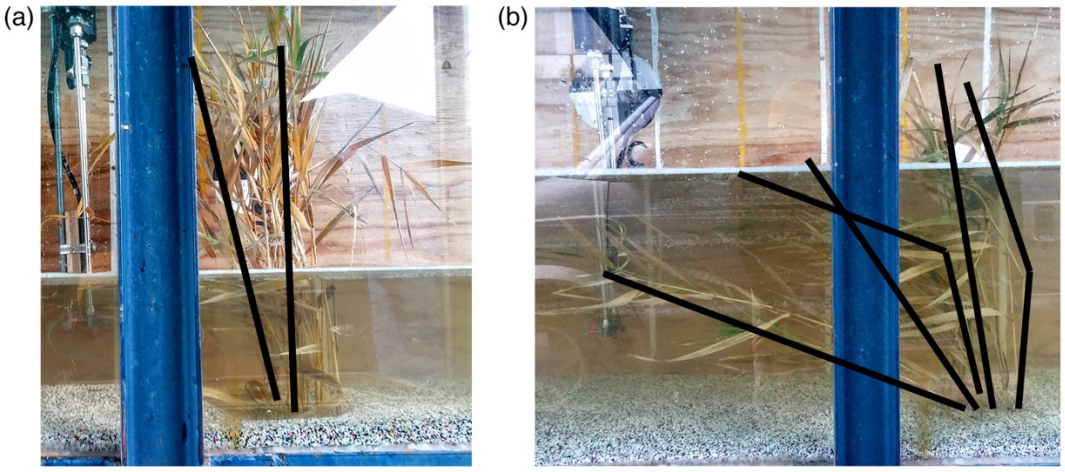

Figure 7: Profile images of patch in low and medium submergence trials. Observed deflection is shown in solid black lines for selected stems within the patch. In the low submergence trial (a), minimal stem deflection occurred. In the medium submergence trial (b), approximately 75% of the patch deflected to below the surface of the water.

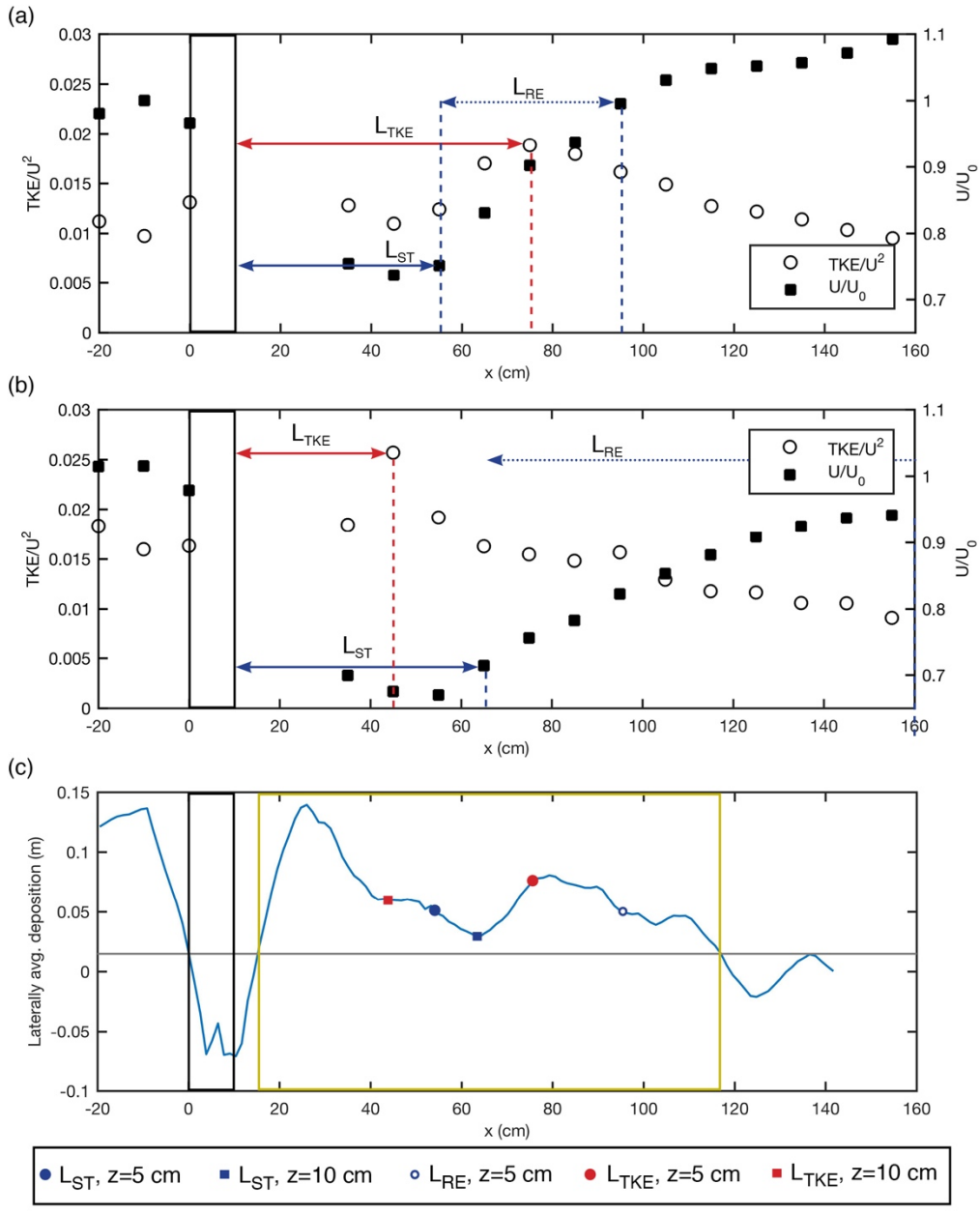

Figure 8: Medium submergence depth trial flow field at 5 cm and 10 cm above the bed and laterally averaged deposition data. In (a), measurements collected along the centerline at 5 cm above the bed are shown and in (b) measurements collected along the centerline at 10 cm above the bed are shown. In both (a) and (b) velocities are normalized by U_0 and TKE values are normalized by local velocity values. Length scale L_{ST} is shown with a dark solid blue arrow and L_{RE} is shown with a dark blue dotted arrow. The length scale L_{TKE} is shown with a red arrow. Dotted vertical lines show the streamwise location, x, of the length scale. In (c) laterally averaged discharge across the experimental area is shown with the wake depositional region outlined in a solid yellow box. A grey line shows the mean of the upstream laterally averaged deposition, used as a datum for distinguishing deposition downstream of patch. A solid blue dot indicates the length scale of L_{ST} for measurement at 5

cm above the bed and a solid blue square shows L_{ST} for measurement 10 cm above the bed along the streamwise direction. An open blue dot shows the length scale L_{RE} for 5 cm above the bed. L_{RE} at 10 cm above the bed extended beyond the experimental zone. The red dot shows the length scale L_{TKE} for 5 cm above the bed and the red square shows L_{TKE} for 10 cm above the bed. The patch location at x = 0 is shown with solid black lines in all plots.

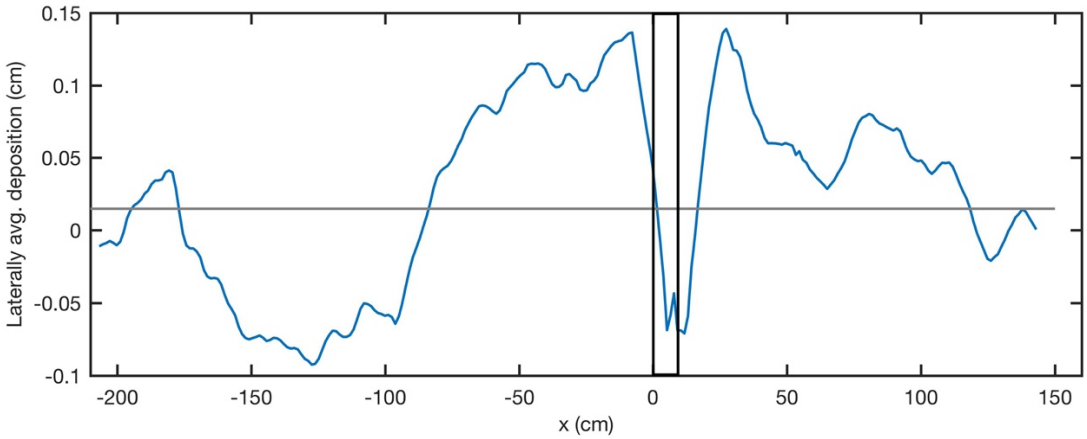

Figure 9: Medium submergence trial laterally averaged deposition upstream and downstream of RCG patch. A grey line indicates average deposition upstream of the patch and is used to distinguish regions of deposition and erosion downstream of patch. Patch location denoted with solid black lines

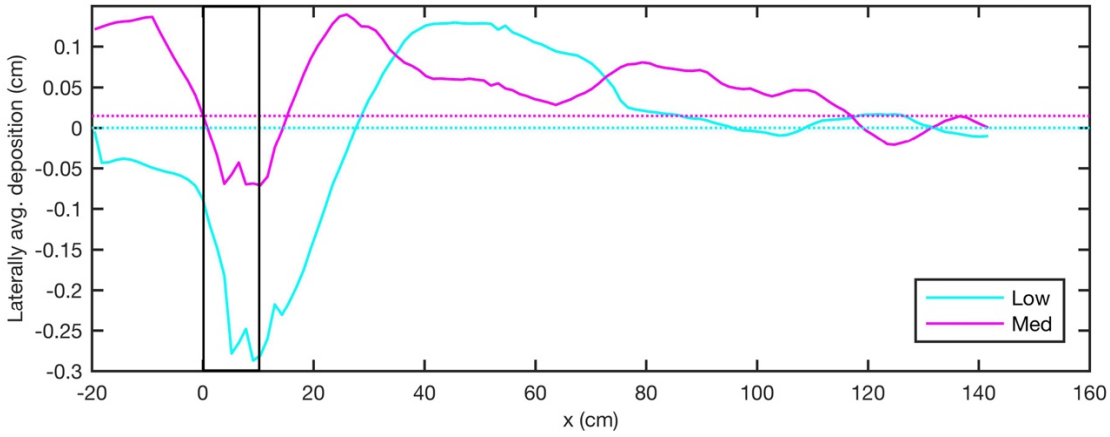

Figure 10: Laterally averaged deposition for both low and medium submergence trials. Dotted lines show upstream average net deposition and are used to characterize regions of deposition and erosion behind the patch. Patch location denoted with solid black lines.

4 Discussion

4.1 Velocity patterns across submergence depths

While velocities were maintained constant between the low and medium submergence trials, discharge changed between trials through the increase of channel depth.

At low submergence, velocities lateral to the RCG patch are higher than medium submergence, initiating a negative feedback loop for patch expansion (Figure 4). High velocities are positively related to high shear which can move finer grain sediments first, leaving an armored layer inhospitable to vegetation growth. Follett and Nepf (2012) found lateral scour to occur around vegetation patches only when a d_{50} of 0.5 mm was used and no scour when d_{50} = 1.8 mm, suggesting that the finer particles moved out of the lateral scour zone. Thus, lateral scour creates an inhospitable environment to vegetation expansion by removing finer, nutrient dense substrate. The prevention of lateral expansion further leads to streamlined propagation behind the patch, as is observed at islands in rivers (Gurnell et al., 2001) and rigid, emergent vegetation patches (Chen et al., 2012b; Follett & Nepf, 2012; Ortiz et al., 2013). Therefore, increased velocity lateral to the

patch, compared to the medium submergence trial, also serves as a positive feedback for downstream, streamlined patch expansion at low submergence.

At medium submergence depth flow passes over the deflected RCG stems and lateral velocities decrease compared to the low submergence trial, generating less lateral scour that inhibits patch expansion (Figure 4). If this trend continues with a fully submerged and deflected patch, lateral velocities may diminish to the degree that fine sediment does not move and lateral vegetation expansion is promoted.

4.2 Near-bed wake across submergence depths

RCG wake zone lengths and peaks in turbulence behind the patch are nearly constant at 5 cm above the bed for both low and medium submerged trials. At this near-bed elevation, the steady wake regions, L_{ST}, and wake recovery regions, L_{RE}, are both equal, indicating that the increase from low to medium submergence depth does not influence near-bed wake zone formation.

4.3 Patterns in wake lengths between depths

At medium submergence, TKE levels indicate that a von Kármán vortex street may have formed near the bed, 5 cm above the bed, but not at 10 cm above the bed, despite higher levels of TKE at the higher, 10 cm, elevation.

At the near-bed measurement, 5 cm above the bed, data show that L_{TKE} occurred within the wake recovery region, L_{RE}. This location of a peak in turbulence, within the wake recovery region and not the steady wake region, has been linked to the formation of a von Kármán vortex street in similar vegetation patch experiments (Zong & Nepf, 2011b). In the wake recovery region, velocity increase due to the joining of the two lateral velocity layers. As these two layers join, turbulence should also then be expected to increase. However, at 10 cm above the bed, L_{TKE} occurs within the steady wake region, L_{ST}, instead of the wake recovery region, L_{RE}, suggesting that the vortex street was not expressed at this elevation in the water column. Rather, it is possible that the velocity passing over the deflected stems created turbulent mixing earlier in the wake zone than at the 5 cm elevation. Indeed, as submergence level increase from partially submerged to fully submerged, the highest levels of turbulence have been found to travel up in the water column, away from the bed and toward the top of the vegetation canopy (Fairbanks & Diplas, 1998). This explains the higher peak in turbulence at 10 cm above the bed compared to 5 cm above the bed, despite evidence of a vortex street.

As submergence increased between trials, wake zone characteristics also became less distinguished. At 5 cm above the bed, a clear wake zone could be identified that was identical to the wake zone lengths behind the RCG patch at low submergence levels. However, at 10 cm above the bed the

steady wake region, L_{ST}, was 10 cm longer than the near-bed location and the wake recovery region, L_{RE}, extended beyond the experimental zone rather than ending at x = 95 cm as the low submergence trial showed. Therefore, velocities within the wake at 10 cm above the bed never returned to upstream velocity levels. Deflected vegetation and the vertical velocity traveling over these stems likely kept velocities lower than the free-stream velocities at 10 cm above the bed while deflected stems. Additionally, Wilson et. al. (2003) found that the foliage on the top of flexible vegetation prevented turbulent mixing between the canopy layer and the near-bud surface area within the water column. The RCG blades, which were thicker near the top of the vegetation, blocked turbulent mixing between the 5cm and 10 cm depths. Thus, the biomechanical structure of the RCG vegetation induced a feedback in the hydraulics that shielded the near-bed (5 cm) region hydraulics from the altered flow field caused by deflected vegetation higher in the water column (10 cm).

4.4 Depositional patterns across submergence depths

In the low submergence depth trial, a sustained peak in wake region deposition serves as a positive feedback for streamlined patch expansion (Figure 5b). The deposition occurs due to the presence of a wake region of diminished velocity, higher lateral velocities, and no canopy shear turbulence

due to deflection of stems. Here, deposition patterns reflect wake structure. At the end of the steady wake region, L_{ST}, where velocities are beginning to increase, laterally averaged deposition begins to decrease. In the wake recovery region, L_{RE}, velocity begins to increase as lateral velocity layers (U_{LAT}) rejoin and initiate the von Kármán vortex street (Zong & Nepf, 2011b). At the peak of turbulence, L_{TKE}, deposition diminishes more rapidly than before the peak. The deposition continues until the end of the wake recovery region where zero laterally averaged deposition was observed. These results are consistent with Chen et. al (2012b), who reported enhanced deposition within the steady wake region behind an emergent patch of rigid vegetation, as well as regions of diminished deposition where velocities and turbulence increased. Ortiz et. al. (2013) also found that deposition decreases in regions of elevated turbulence despite having lower velocities, as was observed between L_{TKE} and L_{RE} in this study. The slower flow in the steady wake region, U_W, postpones the onset of the vortex street and allows particles to deposit (Chen et al., 2012b), while the faster lateral velocities move finer sediment. Therefore, at low submergence levels, RCG patches can likely expand successfully in the downstream direction where deposition occurs in the wake of patches, which also corresponds to location of enhanced nutrient concentrations that are ideal for seedling growth (Follett & Nepf, 2012; Gurnell et al., 2001; K. Sand-Jensen & Madsen, 1992).

Medium trial results show depositional patterns that serve as negative feedbacks for streamlined Reed Canarygrass expansion, but potential positive feedbacks for lateral expansion. First, the initial peak of patch-induced deposition in the lee of the RCG patch in the medium submerged trial is shorter in length than in the low submergence trial (Figure 10). This depositional peak (between x = 15 cm to x = 63 cm) was contained within the steady wake region, $L_{ST,}$ found at both 5 cm and 10 cm measurements above the bed. In contrast, the low trial depositional peak continued to the end of the wake recovery region. The second peak in laterally averaged deposition behind the patch at medium submergence (x = 65 cm to x = 118 cm) is distributed more evenly across the width of the channel than all other wake-zone depositional peaks where deposition was concentrated along the centerline (Figure 6). Therefore, it is assumed that this peak in deposition is caused by different sediment transport mechanisms, similar to those that caused regions of erosion and deposition in front of the RCG patch at medium submergence.

Because wake lengths were identical between the two trials at 5 cm above the bed, yet depositional patterns immediately behind the patch differed between trials, wake characteristics at this near-bed elevation do not solely control deposition within the wake for this species as submergence increases. Instead, wake zone lengths higher in the water column (10 cm elevation)

show evidence of a vertical velocity component over the deflected stems introduced through the plant's biomechanical structure that may have contributed to the drop in deposition seen at x = 63 cm in the medium submergence trial (Figure 10). This result is consistent with Ortiz et al. (2013), who found in fully submerged conditions over flexible vegetation, no wake zone deposition or evidence of a von Kármán vortex street downstream occurred, which they attributed to a fully three-dimensional flow adjustment around the patch despite formation of lateral velocity layers and slower wake zone flow. While a small peak in deposition did occur at medium submergence, it is shorter than the peak in deposition in the low trial.

Lateral scour was diminished in the medium submergence trial compared to the low trial, suggesting the possibility of a potential positive feedback for patch expansion as submergence increases (Figure 6b). As a portion of the patch became fully deflected in the medium submergence trial and velocity traveled over a portion of the canopy, normalized velocity decreased laterally to the patch compared to velocities lateral to the patch at low submergence. As lateral velocities decrease, fine grain sediments are left on the bed lateral to the patch. It may be possible that as the patch becomes fully submerged, lateral velocities will decrease further and allow for vegetation growth laterally. Shi et al. (2016) found that the difference in deposition between the wake and lateral regions depends on the ratio of wake and lateral channel shear

velocities. Specifically, the lateral velocities must be above a critical shear velocity and the wake velocities below this critical shear velocity for deposition to diverge between lateral and wake regions. If velocities are lower in the open channel, less resuspension occurs. The lack of lateral resuspension thus may also contribute to the smaller depositional area behind the patch, as there would be a smaller feed of sediment from the open channel to this region. Indeed, observations of sediment movement during the experiment revealed lateral scour contributing directly to wake deposition.

The reduced lateral scour feedback could also be enhanced by greater stem deflection. A single stem deflected (became nearly horizontal) within approximately 10 cm of the bed on the left side of the patch. The greater streamlining of this plant may have prevented stem-scale turbulence from generating within the patch and continuing around the plant that would contribute to scour (Zong & Nepf, 2010). The deflected stem may also have shielded the bed against lateral velocities and decreased the free-stream velocity near the bed (Koch, 1994). Therefore, as stems become deflected to positions near the bed, lateral scour may continue to reduce.

The generation of canopy shear over fully deflected stems generates additional turbulence in the wake region that inhibits deposition and serves as a negative feedback for streamlined patch expansion. At 10 cm above the bed, turbulent kinetic energy peaked at x = 45 cm, before the end of the

steady wake region (x = 65 cm) likely due to vertical shear over submerged and deflected stems. It is proposed that this turbulence maintains particles in suspension, inhibiting deposition in the wake region. In previous submerged, flexible vegetation studies, the wake zone deposition diminished to zero as submergence increased to fully flow over the canopy (Ortiz et al., 2013). Therefore, the wake characteristics changed differed between trials despite the same velocity entering the patch. Chen, Jiang and Nepf (2013) suggest that the degree of submergence is the dominant control on wake flow dynamics. A portion of the patch remained emergent (approximately 25% of the stems) and thus the degree of submergence remained lower than a fully deflected plant, maintaining diminished velocity closer to the bed that led to a small amount of deposition in the wake region (Figure 8c). Therefore, as submergence increases, a negative feedback for streamlined patch expansion also increases.

5 Conclusion

A physical model was constructed to investigate the hydraulic and bedform evolution feedbacks of a mid-channel Reed Canarygrass patch under low and medium submergence conditions. It was found that as submergence increases, positive feedbacks for patch expansion decrease. At low

submergence depths, positive feedbacks for streamlined patch expansion include deposition behind the patch and high lateral velocities. Both of these feedbacks promote longitudinal deposition streamlined with the patch. Lateral scour serves as a negative feedback for lateral expansion at the low submergence level. At medium submergence, negative feedbacks are seen that inhibit streamlined patch expansion. The introduction of vertical shear over a portion of stems that had become deflected induces high levels of turbulence closer to the vegetation patch in the wake zone and reduces deposition of sediment. However, a decrease in lateral velocities due to velocity traveling over portions of the canopy may promote patch expansion laterally, suggesting a positive mechanism for RCG patch expansion as submergence increases further. Stem deflection close to the bed may also promote vegetation expansion, particularly in regions of higher velocity such as lateral to the plant. The deflected stems act to shield the bedform from higher velocities, thus preventing movement of finer particles.

The discussion presented here is meant to be a starting point for further investigation of feedbacks contributing to the promotion and inhibition of RCG invasions in the wetted channel. A more complete analysis of the progression from low to high submergence levels would provide more robust understanding of the changes in bedform over time, with emphasis on the feedbacks of RCG patches under full submergence.

These data contribute to a relatively unstudied aspect of the spread of this invasive species within stream ecosystems that has significant implications for management strategies. For instance, managers concerned with RCG expansion in rivers where depth will not increase over the height of the plants should expect potential streamlined patch expansion. Removal of these RCG vegetation stands may prevent further spread within the channel. Results here also suggest that in medium submergence conditions, streamlined patch expansion is less likely. Therefore, managers may see less of an aggressive invasion of water levels are at medium submergence. This information could help managers prioritize which patches of RCG to remove first, and which patches may not be spread due as quickly due to feedbacks induced by hydraulics and bedform. By understanding the morphological and hydraulic feedbacks of RCG patches in the wetted channel as submergence level changes, it may be possible to predict the impacts a changing hydrological regime may have upon expansion of the species.

6 Bibliography

Abt, S. R., Clary, W. P., & Thornton, C. I. (1994). Sediment deposition and entrapment in vegetated streambeds. *Journal of Irrigation and Drainage Engineering*, *120*(6), 1098–1111.

Apfelbaum, S. I., Sams, C. E., & others. (1987). Ecology and control of reed canary grass (Phalaris arundinacea L.). *Natural Areas Journal*, *7*(2), 69–74.

ArcGIS Desktop. (2013). Redlands, CA: Environmental Systems Research Institute.

Ball, D. J., Stansby, P. K., & Alliston, N. (1996). Modelling shallow water flow around pile groups. *Proc. Inst. Civ.Engrs Wat., Marit. Energy*, *118*, 226–236.

Barnes, W. J. (1999). The Rapid Growth of a Population of Reed Canarygrass (Phalaris arundinacea L.) and Its Impact on Some Riverbottom Herbs. *Journal of the Torrey Botanical Society*, *126*(2), 133. http://doi.org/10.2307/2997289

Bouma, T. J., van Duren, L. A., Temmerman, S., Claverie, T., Blanco-Garcia, A., Ysebaert, T., & Herman, P. M. J. (2007). Spatial flow and sedimentation patterns within patches of epibenthic structures: Combining field, flume and modelling experiments. *Continental Shelf Research*, *27*(8), 1020–1045. http://doi.org/10.1016/j.csr.2005.12.019

Cellino, M., & Lemmin, U. (2004). Influence of Coherent Flow Structures on the Dynamics of Suspended Sediment Transport in Open-Channel Flow. *Journal of Hydraulic Engineering*, *130*(11), 1077–1088. http://doi.org/10.1061/(ASCE)0733-9429(2004)130:11(1077)

Chen, Z., Jiang, C., & Nepf, H. (2013). Flow adjustment at the leading edge of a submerged aquatic canopy: FLOW ADJUSTMENT THROUGH A SUBMERGED CANOPY. *Water Resources Research*, *49*(9), 5537–5551. http://doi.org/10.1002/wrcr.20403

Chen, Z., Ortiz, A., Zong, L., & Nepf, H. (2012a). The wake structure behind a porous obstruction and its implications for deposition near a finite patch of emergent vegetation. *Water Resources Research*, *48*(9), W09517. http://doi.org/10.1029/2012WR012224

Chen, Z., Ortiz, A., Zong, L., & Nepf, H. (2012b). The wake structure behind a porous obstruction and its implications for deposition near a finite patch of emergent vegetation. *Water Resources Research*, *48*(9), W09517. http://doi.org/10.1029/2012WR012224

Coops, H., & Van Der Velde, G. (1995). Seed dispersal, germination and seedling growth of six helophyte species in relation to water-level zonation. *Freshwater Biology*, *34*(1), 13–20. http://doi.org/10.1111/j.1365-2427.1995.tb00418.x

Corenblit, D., Baas, A. C. W., Bornette, G., Darrozes, J., Delmotte, S., Francis, R. A., … Steiger, J. (2011). Feedbacks between geomorphology and biota controlling Earth surface processes and landforms: A review of foundation concepts and current understandings. *Earth-Science Reviews*, *106*(3–4), 307–331. http://doi.org/10.1016/j.earscirev.2011.03.002

Corenblit, D., Tabacchi, E., Steiger, J., & Gurnell, A. M. (2007). Reciprocal interactions and adjustments between fluvial landforms and vegetation dynamics in river corridors: A review of complementary approaches. *Earth-Science Reviews*, *84*(1–2), 56–86. http://doi.org/10.1016/j.earscirev.2007.05.004

Curran, J. C., & Hession, W. C. (2013). Vegetative impacts on hydraulics and sediment processes across the fluvial system. *Journal of Hydrology*, *505*, 364–376. http://doi.org/10.1016/j.jhydrol.2013.10.013

Ehrenfeld, J. G. (2010). Ecosystem Consequences of Biological Invasions. *Annual Review of Ecology, Evolution, and Systematics*, *41*(1), 59–80. http://doi.org/10.1146/annurev-ecolsys-102209-144650

Fairbanks, J. D., & Diplas, P. (1998). Turbulence characteristics of flows through partially and fully submerged vegetation. In *Proc., Wetlands Engineering and River Restoration Conf.: Engineering Approaches to Ecosystem Restoration* (pp. 865–870). Retrieved from http://ascelibrary.org/doi/pdf/10.1061/40382(1998)144

Fei, S., Phillips, J., & Shouse, M. (2014). Biogeomorphic Impacts of Invasive Species. *Annual Review of Ecology, Evolution, and Systematics*, *45*(1), 69–87. http://doi.org/10.1146/annurev-ecolsys-120213-091928

Folkard, A. M. (2005). Hydrodynamics of model Posidonia oceanica patches in shallow water. *Limnology and Oceanography*, *50*(5), 1592–1600.

Folkard, A. M. (2011a). Flow regimes in gaps within stands of flexible vegetation: laboratory flume simulations. *Environmental Fluid Mechanics*, *11*(3), 289–306. http://doi.org/10.1007/s10652-010-9197-5

Folkard, A. M. (2011b). Flow regimes in gaps within stands of flexible vegetation: laboratory flume simulations. *Environmental Fluid Mechanics*, *11*(3), 289–306. http://doi.org/10.1007/s10652-010-9197-5

Follett, E. M., & Nepf, H. M. (2012). Sediment patterns near a model patch of reedy emergent vegetation. *Geomorphology*, *179*, 141–151. http://doi.org/10.1016/j.geomorph.2012.08.006

Goring, D. G., & Nikora, V. I. (2002). Despiking Acoustic Doppler Velocimeter Data. *Journal of Hydraulic Engineering*, *128*(1), 117–126.

Green, J. C. (2005). Further comment on drag and reconfiguration of macrophytes. *Freshwater Biology*, *50*(12), 2162–2166. http://doi.org/10.1111/j.1365-2427.2005.01470.x

Gurnell, A. M., Bertoldi, W., & Corenblit, D. (2012). Changing river channels: The roles of hydrological processes, plants and pioneer fluvial landforms in humid temperate, mixed load, gravel bed rivers. *Earth-Science Reviews*, *111*(1–2), 129–141. http://doi.org/10.1016/j.earscirev.2011.11.005

Gurnell, A. M., Petts, G. E., Hannah, D. M., Smith, B. P., Edwards, P. J., Kollmann, J., … Tockner, K. (2001). Riparian vegetation and island formation along the gravel-bed Fiume Tagliamento, Italy. *Earth Surface Processes and Landforms*, *26*(1), 31–62. http://doi.org/10.1002/1096-9837(200101)26:1<31::AID-ESP155>3.0.CO;2-Y

Henry, C. P., & Amoros, C. (1996). Are the banks a source of recolonization after disturbance: an experiment on aquatic vegetation in a former channel of the Rhone River. *Hydrobiologia*, *330*, 151–162.

Hickin, E. J. (1984). Vegetation and river channel dynamics. *The Canadian Geographer/Le Géographe Canadien*, *28*(2), 111–126.

Julien, Pierre Y. (2002). *River mechanics*. Cambridge ; New York: Cambridge University Press.

Kellogg, C. H., Bridgham, S. D., & Leicht, S. A. (2003). Effects of Water Level, Shade and Time on Germination and Growth of Freshwater Marsh Plants along a Simulated Successional Gradient. *Journal of Ecology*, *91*(2), 274–282.

Koch, E. (1994). Hydrodynamics, diffusion-boundary layers and photosynthesis of the seagrasses Thalassia testudinum and Cymodocea nodosa. *Marine Biology*, *118*(4), 767–776.

Lavergne, S., & Molofsky, J. (2004). Reed Canary Grass (*Phalaris arundinacea*) as a Biological Model in the Study of Plant Invasions. *Critical Reviews in Plant Sciences*, *23*(5), 415–429. http://doi.org/10.1080/07352680490505934

Leica Cyclone. (n.d.). (Version 9.1.1). San Ramon, California: Leica Geosystems.

Luhar, M., & Nepf, H. M. (2013). From the blade scale to the reach scale: A characterization of aquatic vegetative drag. *Advances in Water Resources*, *51*, 305–316. http://doi.org/10.1016/j.advwatres.2012.02.002

Martinez, A. E., & McDowell, P. F. (2016). Invasive Reed Canarygrass (*Phalaris arundinacea*) and Native Vegetation Channel Roughness. *Invasive Plant Science and Management*, *9*(1), 12–21. http://doi.org/10.1614/IPSM-D-15-00046.1

Nepf, H. M. (1999). Drag, turbulence, and diffusion in flow through emergent vegetation. *Water Resources Research*, *35.2*, 479–489.

Nepf, H. M. (2012a). Flow and Transport in Regions with Aquatic Vegetation. *Annual Review of Fluid Mechanics*, *44*(1), 123–142. http://doi.org/10.1146/annurev-fluid-120710-101048

Nepf, H. M. (2012b). Hydrodynamics of Vegetated Channels. *Journal of Hydraulic Research*, *50*(3), 262–279.

Nepf, H. M., & Vivoni, E. R. (2000). Flow structure in depth-limited, vegetated flow. *Journal of Geophysical Research*, *105*(C12), 28,547-28,557.

Nicolle, A., & Eames, I. (2011). Numerical study of flow through and around a circular array of cylinders. *Journal of Fluid Mechanics*, *679*, 1–31. http://doi.org/10.1017/jfm.2011.77

Odling-Smee, F. J., Feldman, M. W., & Laland, K. N. (2003). *Niche Construction: the Neglected Process in Evolution*. Princeton, NJ: Princeton Univ. Press.

Ortiz, A. C., Ashton, A., & Nepf, H. (2013). Mean and turbulent velocity fields near rigid and flexible plants and the implications for deposition. *Journal of Geophysical Research: Earth Surface*, *118*(4), 2013JF002858. http://doi.org/10.1002/2013JF002858

Paveglio, F. L., & Kilbride, K. M. (2000). Response of Vegetation to Control of Reed Canarygrass in Seasonally Managed Wetlands of Southwestern Washington. *Wildlife Society Bulletin*, *28*(3), 730–740.

Poggi, D., Katul, G. G., & Albertson, J. D. (2004). A note on the contribution of dispersive fluxes to momentum transfer within canopies. *Boundary-Layer Meteorology*, *111*(3), 615–621.

Pope, S. B. (2000). *Turbulent Flows*. New York: Cambridge University Press.

Sand-Jensen, K. (2003). Drag and reconfiguration of freshwater macrophytes. *Freshwater Biology*, *48*(2), 271–283.

Sand-Jensen, K., & Madsen, T. V. (1992). Patch dynamics of the stream macrophyte, <i>Callitriche cophocarpa<i>. *Freshwater Biology*, *27*, 277–282.

Sand-Jensen, K., & Mebus, J. R. (1996). Fine-Scale Patterns of Water Velocity within Macrophyte Patches in Streams. *Oikos*, *76*(1), 169. http://doi.org/10.2307/3545759

Shi, Y., Jiang, B., & Nepf, H. M. (2016). Influence of particle size and density, and channel velocity on the deposition patterns around a circular patch of model emergent vegetation: VEGETATION PATCH ON DEPOSITION PATTERNS. *Water Resources Research*, *52*(2), 1044–1055. http://doi.org/10.1002/2015WR018278

Shields, A. (1936). Anwendung der Aenlichkitsmechanik und der Turbulenzforshung auf die Geschiebebewegung. *Berlin: Mitteilungen Der Prevssischen Versuchsanstalt Fur Wasserbau Und Schiffbau.*

Sukhodolov, A. (2005). Comment on drag and reconfiguration of macrophytes. *Freshwater Biology*, *50*(1), 194–195. http://doi.org/10.1111/j.1365-2427.2004.01296.x

Tsujimoto, T. (1999). Fluvial processes in streams with vegetation. *Journal of Hydraulic Research*, *37*(6), 789–803. http://doi.org/10.1080/00221689909498512

Västilä, K., Järvelä, J., & Aberle, J. (2013). Characteristic reference areas for estimating flow resistance of natural foliated vegetation. *Journal of Hydrology*, *492*, 49–60. http://doi.org/10.1016/j.jhydrol.2013.04.015

Wahl, T. L. (n.d.). WinADV (Version 1.5). Denver, Colorado: Water Resources Research Laboratory U.S. Bureau of Reclamation.

Washington State Department of Ecology. (n.d.). Non-native Invasive Freshwater Plants - Reed Canarygrass (Phalaris arundinacea) - Technical Information. Retrieved February 28, 2015, from http://www.ecy.wa.gov/programs/wq/plants/weeds/aqua011.html

Wilson, C. A., Hoyt, J., & Schnauder, I. (2008). Impact of foliage on the drag force of vegetation in aquatic flows. *Journal of Hydraulic Engineering*, *134*(7), 885–891.

Wilson, C. A. M. E., T. Stoesser, Bates, P. D., & A. Batemann Pinzen. (2003). Open Channel Flow through Different Forms of Submerged Flexible Vegetation. *Journal of Hydraulic Engineering*, *129*(11), 847–853.

Zong, L., & Nepf, H. (2010). Flow and deposition in and around a finite patch of vegetation. *Geomorphology*, *116*(3–4), 363–372. http://doi.org/10.1016/j.geomorph.2009.11.020

Zong, L., & Nepf, H. (2011a). Spatial distribution of deposition within a patch of vegetation: DEPOSITION PATTERN WITHIN A PATCH. *Water Resources Research*, *47*(3), n/a-n/a. http://doi.org/10.1029/2010WR009516

Zong, L., & Nepf, H. (2011b). Vortex development behind a finite porous obstruction in a channel. *Journal of Fluid Mechanics*, *691*, 368–391. http://doi.org/10.1017/jfm.2011.479

7 APPENDIX

7.1 Accuracy and error

Velocity error is minimal for both low and medium submergence trials. Velocity errorbars show the magnitude of the resultant formed using the individual RMS values for each x, y, and w component (Figure 11). A minimum error of 1.8 cm/s and 2.2 cm/s and maximum error of 6.8 cm/s and 3.8 cm/s is found for low trial 3 and medium trial 1 respectively.

Final point cloud density within the experiment zone ranged from 0.001 points/m^2 to 0.007 points/m^2 for all scans. Diagnostics of registration error were exported from Leica Cyclone software (*Leica Cyclone*, n.d.) for the *pre* and *post* scans (each containing 4 individual scans as described above). Registration was performed using target-to-target registration using 5 targets (Figure 12). Smoothing of the *pre* scan DEMs was performed first by the mean value of a 30 cell extent to the output cells. Next, the raster was resampled to return to the same cell size as *post* scan DEM. There is an uncaptured error associated with this process. Horizontal error from registration is assumed to be negligible as it ranges in 0.003 m – 0.006 m and the resolution of hydrological data is +/- 5-10 cm within the experimental zone. A horizontal RMSE of 0.001 cm is assumed to not have an impact on the locations of the wake length scale characteristics upon the depositional data. Vertical error for bedform data is described by the square root of the sum of squares of both the vertical errors in the *post* scan and the *pre* scans

(Tables 3 - 6). The total vertical error is 0.001 m for both trials. This error may impact the vertical distances from the datum used to find the laterally averaged discharge.

7.2 Sediment entrainment calculations

Using the depth-slope equation and assuming steady, uniform flow, the boundary shear stress, τ_0, is defined as

$$\tau_0 = \rho g R s$$

where ρ is the density of water, g is gravitational acceleration, R is the hydraulic radius of the flume, and s is the slope (0.0007). Using the boundary shear stress, the dimensionless critical Shields stress was calculated using

$$\tau_c{}^* = \frac{\tau_0}{(\rho_s - \rho) g D_{50}}$$

where ρ_s is the density of modeled sediment (1500 kg/m^3), and D_{50} is 0.0014 m (Shields, 1936). τ_c* is found to be 0.132. The particle Reynolds number is calculated using

$$\boldsymbol{Re^*} = \frac{\boldsymbol{u^* D_{50}}}{\boldsymbol{\upsilon}}$$

where u^* is the shear velocity and υ is the kinematic viscosity at 10 degrees Celsius, we compare the $\tau_c{}^*$ calculated using quartz sand with a density of 2650 kg/m^3 of 0.04 with the $\tau_c{}^*$ value for the modeled sediment. The $\tau_c{}^*$ value for the model sediment lies above the threshold for entrainment and will

therefore move at the model flows (Figure 13). A model grain size distribution was created by mixing three size classes of plastic material with d_{50} grain sizes of 0.7 mm, 1.2 mm, and 1.4 mm. The mixture consisted of 1 to 4 parts of 0.7 mm and 1.2 mm size classes and 1 to 2 parts ratio for the 1.4 mm grain size (Figure 14). No upstream sediment feed was introduced.

7.3 Reed Canarygrass field observations and data collection

RCG morphological parameters used in calculations were obtained during field survey work in July 2015 at the H.J. Andrews Experimental Forest. Research assistants with the Engineering and Informatics Summer Institute (EISI) REU program performed the data collection (table 7). The 5% to 95% confidence interval for vegetation heights is 43.1 cm to 168 cm (table 8). Field observations were also made at an unnamed tributary to Oak Creek in Corvallis, OR. Plant samples used in flume trials were gathered from the Oak Creek tributary location.

7.4 Feedback dependence on frontal area

The feedbacks presented for each trial are all dependent upon vegetation density. Because the methods for assigning frontal area values to flexible, mechanically complex vegetation are problematic (Västilä, Järvelä, & Aberle, 2013), two methods were used to represent the minimum and

maximum possible frontal areas, a_1 and a_2 respectively. These two values are compared with previous vegetation patch experiments to determine a more appropriate frontal area and solid volume fraction for RCG than the minimum and maximum values. First, previous research suggests that a minimum solid volume fraction for RCG ($\phi_1 = 0.02$) would likely not produce a von Kármán vortex street. Nicolle and Eames (2011) found that no steady wake region developed with characteristic patch-scale vortices in patch solid volume fractions less than 0.05. Zong and Nepf (2011) conducted a flume study with a slightly higher solid volume fraction ($\phi = 0.04$) using rigid, emergent cylinders and found an L_{ST} of 80 cm and an L_{RE} of 140 cm. Both length scales are longer than length scales found in this study, suggesting a greater bleed flow through the vegetation occurred to create a longer wake zone. Thus, it is likely that using only stem diameter as the plant characteristic area underestimates patch density. The highest density examined by Zong and Nepf (2011), ($a = 0.77$, $\phi = 0.36$), was near the density calculated using all foliage area for RCG ($a = 1.13$ cm^{-1}, $\phi = 0.26$). However, Zong and Nepf found no steady wake region ($L_{ST} = 0$ cm), similar to wake behavior behind a solid cylinder. Numerical modeling at similar solid volume fractions also shows little to no wake region (Nicolle & Eames, 2011). RCG patches at both submergence depths show evidence of a steady wake zone, thus a density calculated using maximum RCG foliage frontal area is likely an overestimate.

Results that show similar wake length scales to the RCG patches investigated here have a solid volume fraction of 0.1 and a frontal area of 0.20 cm^{-1} (Zong & Nepf, 2011b). Comparing results of this investigation to previous research on vegetation patches, it is likely that the frontal area for RCG is closer to 0.20 cm^{-1}, rather than the sparse 0.07 cm^{-1} or dense 1.1 cm^{-1} calculated.

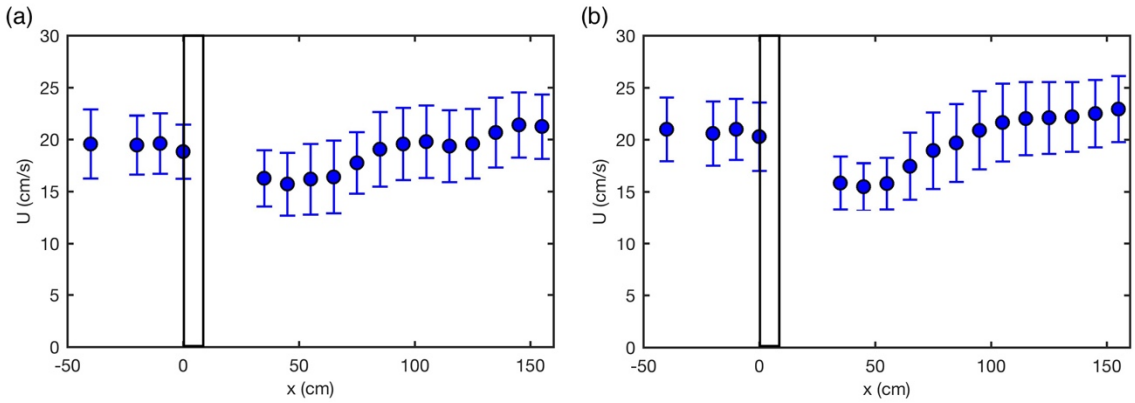

Figure 11: Errorbars for centerline velocity measurements in low and medium submergence trials. The (a) low submergence trial mean error is 2.8 cm/s and (b) medium submergence trial mean error is 2.8 cm/s. Patch location shown with solid black box. Velocity measurements taken at 5 cm elevation above the bed.

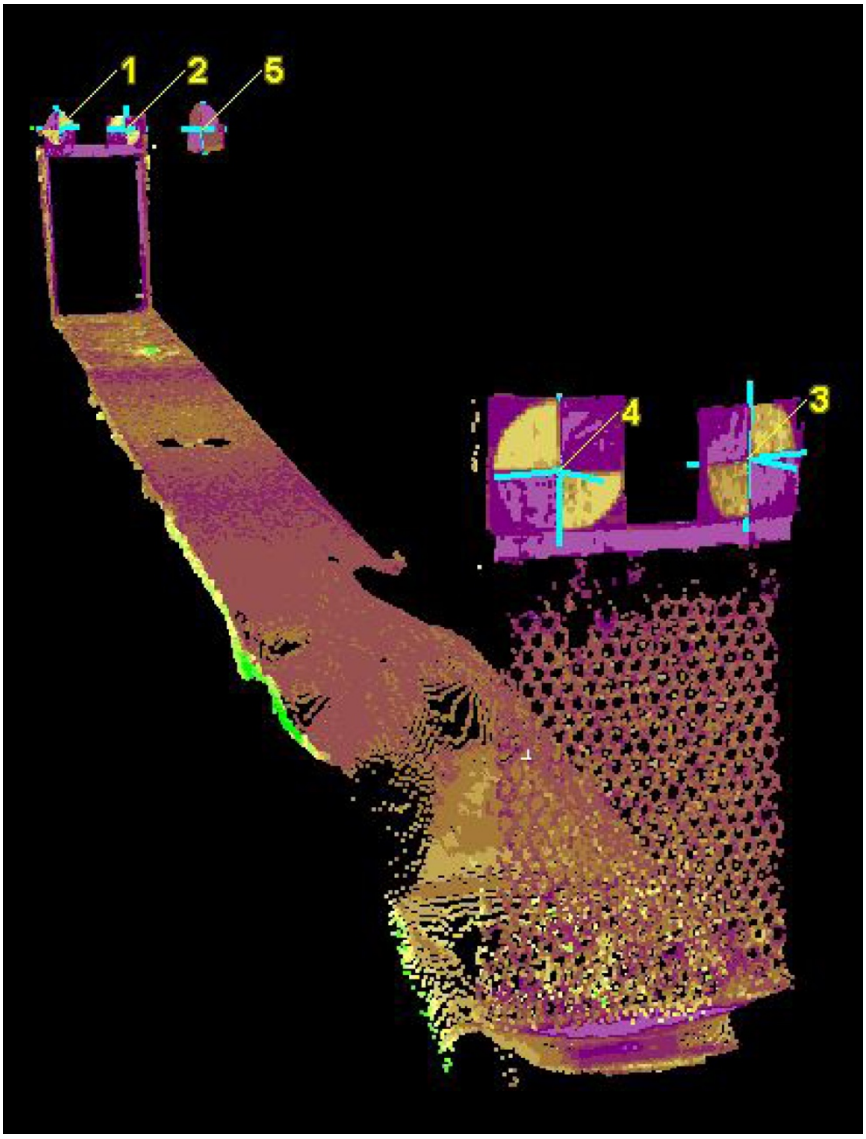

Figure 12: Registration target location for each LiDAR scan. Five targets were used to register the scan. Targets 1-4 were placed at a diagonal on each corner of the flume. Target 5 was placed approximately 6 meters from the head of the flume (the flume was 10 meters in total length). Image is the *post* scan point cloud for the low submergence trial. Circles in the bottom right of image (below targets 3 and 4) are the ends of the diffusion tubes and are thus the upstream end of the flume. The weir was placed below targets 1 and 2.

Table 3: Low trial *pre* LiDAR scan registration errors.

Low Trial PRE LiDAR Scan: Target to Target Registration Summary of Errors (m)			
Statistic	**Total**	**Horizontal**	**Vertical**
AVERAGE	0.002	0.001	0.000
MIN	0.000	0.000	-0.001
MAX	0.003	0.003	0.002
Std Dev	0.001	0.001	0.001
RMSE	0.002	0.002	0.001

Table 4: Low trial *post* LiDAR scan registration errors.

Low Trial POST LiDAR Scan: Target to Target Registration Summary of Errors (m)			
Statistic	**Total**	**Horizontal**	**Vertical**
AVERAGE	0.002	0.001	0.000
MIN	0.000	0.000	-0.002
MAX	0.003	0.003	0.002
Std Dev	0.001	0.001	0.001
RMSE	0.002	0.002	0.001

Table 5: Medium trial *pre* LiDAR scan registration errors.

Medium Trial PRE LiDAR Scan: Target to Target Registration Summary of Errors (m)			
Statistic	**Total**	**Horizontal**	**Vertical**
AVERAGE	0.001	0.001	0.000
MIN	0.000	0.000	-0.002
MAX	0.003	0.003	0.002
Std Dev	0.001	0.001	0.001
RMSE	0.002	0.002	0.001

Table 6: Medium trial *post* LiDAR scan registration errors.

Medium Trial POST LiDAR Scan: Target to Target Registration Summary of Errors (m)			
Statistic	**Total**	**Horizontal**	**Vertical**
AVERAGE	0.001	0.001	0.000
MIN	0.000	0.000	-0.001
MAX	0.003	0.003	0.002
Std Dev	0.001	0.001	0.001
RMSE	0.002	0.001	0.001

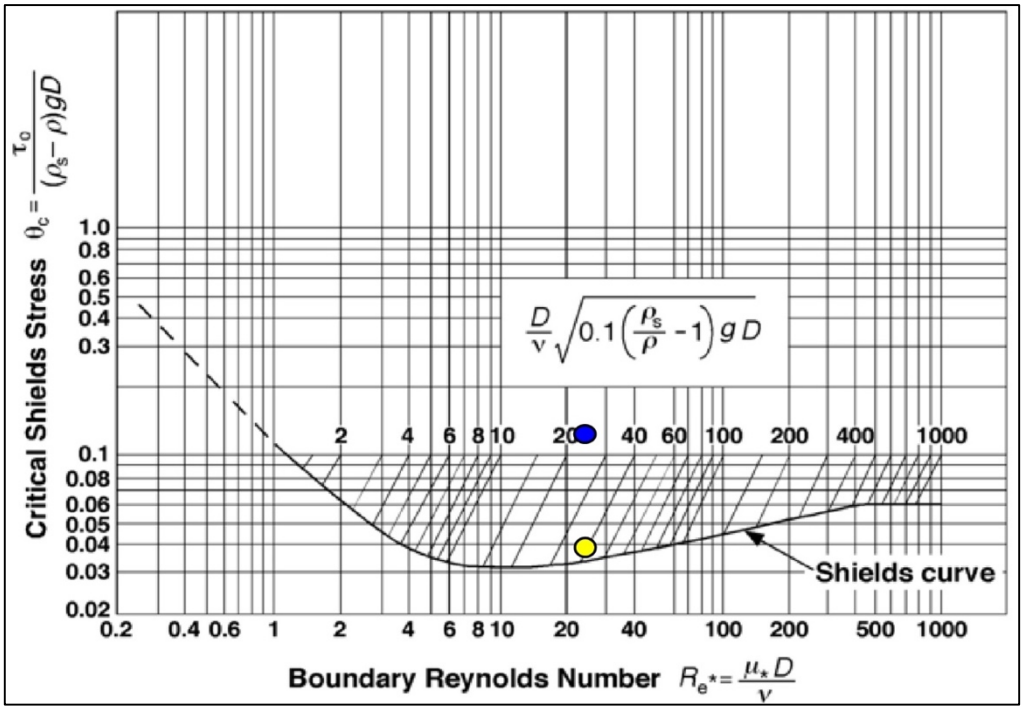

Figure 13: Shields diagram with Shields stress values for modeled sediment. Blue dot indicates calculated value for plastic sediment Shields stress value. Yellow dot indicates quartz sediment calculated Shields number value.

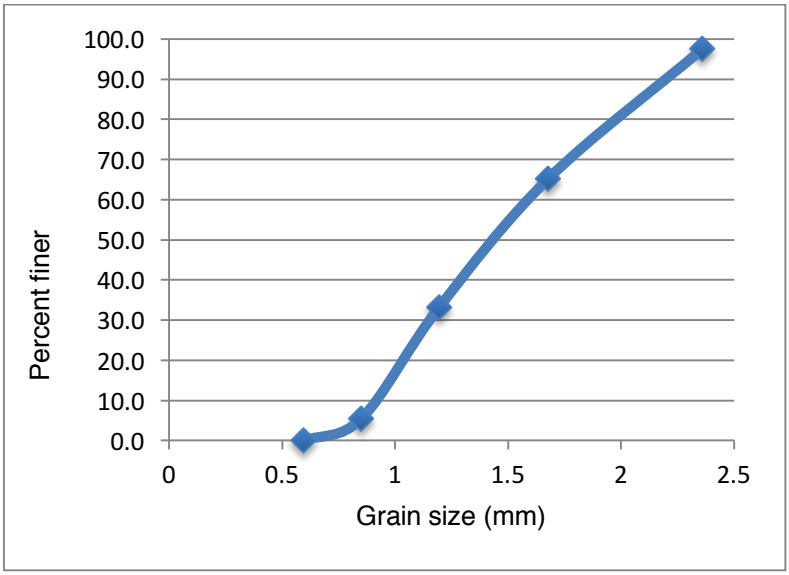

Figure 14: Grain size distribution for modeled sediment mixture.

Table 7: Morphological field survey data of Reed Canarygrass performed at the H.J. Andrews Research Forest, June 2015. Standard deviation from the mean shown in parenthesis.

Measured parameter	**Mean (SD)**
Number of plants per 4 ft^2	93.3 (45.0)
Height (cm)	107 (44.3)
Stem diameter, d (cm)	0.29 (0.08)
Blade width (cm)	1.26 (0.33)
Blade length (cm)	23.4 (4.5)
Number of blades per plant	6 (1.2)

Table 8: RCG height confidence interval from surveyed measurements.

RCG surveyed height confidence interval			
	5%	**95%**	**Mean**
RCG height (cm)	43.1	168	107